Micromechanics of high temperature hydrogen attack

Schl"gl, S.M.; van der Giessen, E.; Schlögl, Sabine M.; Schlogl, SM

Published in:
International Journal for Numerical Methods in Engineering

DOI:
10.1002/nme.299

INTERNATIONAL JOURNAL FOR NUMERICAL METHODS IN ENGINEERING
Int. J. Numer. Meth. Engng 2001; **52**:559–567 (DOI: 10.1002/nme.299)

Micromechanics of high temperature hydrogen attack

Sabine M. Schlögl[*,†] and Erik Van der Giessen[‡]

Micromechanics of Materials Group, Department of Applied Physics, University of Groningen, Nijenborgh 4, 9747 AG Groningen, The Netherlands

SUMMARY

Hydrogen attack is a material degradation process that occurs at elevated temperatures in hydrogen-rich environments, such as found in petrochemical installations. Weldments in components such as reactor vessels are particularly susceptible to hydrogen attack. This paper discusses a multi-scale micromechanics modelling approach in which the chemico-mechanical damage processes at sub-micron scale are coupled to the macroscopic behaviour through a series of size-scale transitions. A simulation of hydrogen attack in a welded reactor serves as an illustration of the approach. Copyright © 2001 John Wiley & Sons, Ltd.

KEY WORDS: micromechanics; fracture; creep; hydrogen

1. INTRODUCTION

With the growing computing capabilities and the development of computational tools, we are witnessing the increased ability to relate fracture properties of materials to their microstructure and the relevant physical phenomena. A well-known example of this is ductile fracture of metals by void nucleation and growth until coalescence (see, e.g. Reference [1] for a review), although many details are still being debated. A somewhat more complex phenomenon is intergranular fracture at high temperatures because this involves a number of different physical mechanisms such as dislocation creep, grain boundary and grain boundary sliding. Nevertheless, computational techniques have been recently developed that allow to describe intergranular crack growth in a granular microstructure on the basis of the elemental physical mechanisms.

A class of still more complex phenomena is that where chemical aspects, in competition with mechanical phenomena, are also playing a major role. One example of this is hydrogen attack (HA). This is a degradation process occurring in steels in a hydrogen-containing atmosphere at temperatures above $\sim 200°C$. Hydrogen atoms can easily diffuse into steel, where at discontinuities, they react with the carbon in the steel to form cavities filled by methane.

*Correspondence to: Sabine M. Schlögl, Micromechanics of Materials Group, Department of Applied Physics, University of Groningen, Nijenborgh 4, 9747 AG Groningen, The Netherlands
†E-mail: S.M.Schloegl@phys.rug.nl
‡E-mail: E.van.der.giessen@phys.rug.nl

Especially along the grain boundaries, these cavities grow due to the relatively high internal methane pressure and possible external loading. The deformation mechanisms involved are grain-boundary diffusion and dislocation creep. When these cavities have grown to sufficiently large sizes, coalescence takes place and microcracks are formed. These microcracks link up and lead to intergranular failure of the component.

Hydrogen attack is a notorious failure mode in the petrochemical industry in reactors for hydrocracking, hydrotreating and similar refinery applications. Thick-walled reactors with diameters of several metres are often manufactured by circumferential welding of forged belts made of 2.25Cr–1Mo steel. This is a bainitic steel containing carbides such as M_7C_3, M_6C and M_2C. Since weldments possess various microstructures that may be more susceptible to hydrogen attack, welds are often critical locations for HA.

There is an obvious interest in understanding and preventing HA, but to date design of such reactors is carried out on the basis of simple empirical data (the so-called Nelson curves). In recent years, however, we have started to develop a micromechanics approach to HA that aims at linking HA failure of, for example, a vessel or reactor to the formation of methane in growing grain boundary cavities. This paper gives a brief exposure of the state-of-the-art, and emphasizes the scale transitions involved. The modelling combines a description of the methane reaction with the mechanics of damage evolution driven by the methane. The resulting continuum model for HA damage at the macroscopic scale is applied to study the damage accumulation in a welded reactor.

2. A MICROMECHANICS APPROACH TO HA

It has been long recognized [2] that the methane pressure is a crucial factor in the lifetime of a component under HA, as this is the main driving force for cavity growth. The susceptibility to hydrogen attack is determined by the microstructure of the steel, especially by its alloy carbides.

The methane pressure depends on the kinetics of methane formation, the dissolution of carbides as well as on the growth of the cavities containing the pressurized methane. Thus, the calculation of the methane pressure is a formidable, coupled problem for which no solution is available at this moment [3]. A common approach is to assume that the chemical reaction and the dissolution are much faster than cavity growth and creep on the time scales of the lifetime of a component (around 20–30 years). As a consequence, the methane pressure p_{CH_4} can be approximated by the equilibrium methane pressure, independent of the associated damage development. Our HA model is therefore split up into two decoupled parts:

- a thermodynamical model to compute the equilibrium methane pressure on the basis of the carbide types and compositions, as a function of temperature;
- a model for the damage accumulation in the material, as driven (mainly) by the methane pressure.

The most recent version of the thermodynamical model can be found in Reference [3]. In the remainder of the present paper, we focus on the mechanical part of the model.

HA involves a number of size scales, and we identify three main ones (Figure 1). The microscopic scale is concerned with individual cavities. At the mesoscopic scale, we are dealing with an aggregate of grains, with a number of grain facets being covered with cavities.

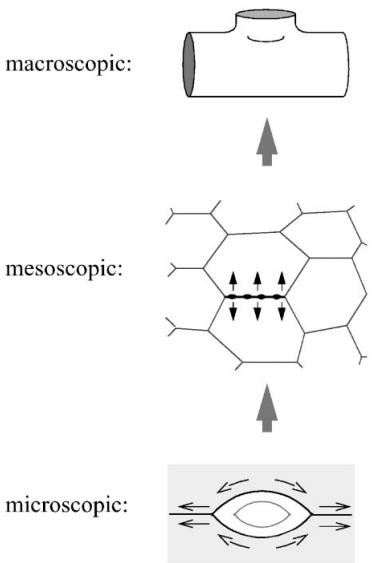

Figure 1. The three size scales considered in the modelling of HA damage.

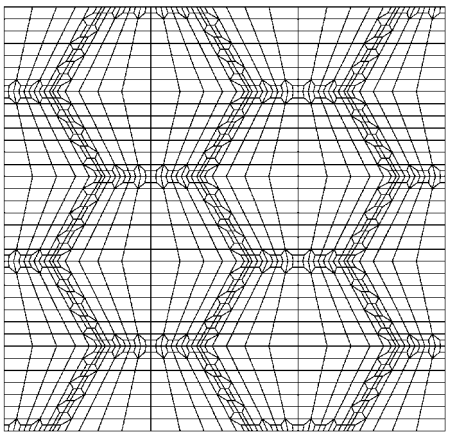

Figure 2. Example of a mesh used for modelling at the mesoscopic scale. The mesh for each hexagonal grain is refined near the grain boundaries. Adjacent grains are connected by interface or cohesive zone elements that account for cavity growth under internal methane pressure.

Finally, the macroscopic scale is the size scale of components at which we can average over many cavities and cavitated facets. Van der Burg *et al.* [4–7] have developed models for each of these length scales as well as the scale transitions between them. A brief, and updated summary, is given in the following subsections.

2.1. Microscopic model

At the microscale, we consider a single grain boundary cavity filled with a gas mixture of hydrogen and methane. Firstly, detailed computations of the growth of a single void subject to an internal gas pressure and a remote stress state have been carried out in Reference [8], by simultaneous creep of the grains and diffusion along the grain boundaries. The coupled numerical simulations were summarized in a set of closed-form approximate relationships for the growth rate of the cavity volume, $\dot{V}$, as a function of the current void radius a and spacing b. Referring to Reference [8] for details, the expression is of the form

$$\dot{V}^{\mathrm{cav}} = \dot{V}^{\mathrm{cav}}_{\mathrm{diff}}(a, b, p_{\mathrm{m}}, \sigma_{\mathrm{n}}, \sigma_{\mathrm{e}}) + \dot{V}^{\mathrm{cav}}_{\mathrm{cr}}(a, b, p_{\mathrm{m}}, \sigma_{\mathrm{m}}, \sigma_{\mathrm{e}}) \tag{1}$$

where p_{m} is the internal pressure inside the cavity and which for HA is

$$p_{\mathrm{m}} = p_{\mathrm{CH_4}} + p_{\mathrm{H_2}} \tag{2}$$

with $p_{\mathrm{CH_4}}$ from the thermodynamical model. The other stresses in (1) represent the stress state remote to the cavity: σ_{n} is the stress normal to the grain boundary facet, σ_{m} the hydrostatic

stress component and σ_e the effective Mises stress. The creep contribution $\dot{V}_{cr}^{cav}$ depends on the creep properties appearing in the power law

$$\dot{\varepsilon}_e^C = B(T)\sigma_e^n \tag{3}$$

i.e. the creep exponent n and the temperature-dependent parameter $B(T)$. This isotropic model for the Von Mises equivalent strain-rate $\dot{\varepsilon}_e$ is regarded to give a mean description of the steady-state creep in grains averaged over many grains. The diffusive contribution $\dot{V}_{diff}^{cav}$ depends on a temperature-dependent grain boundary diffusion parameter $\mathscr{D}(T)$ as well as on a stress- and temperature-dependent length parameter which is defined as [9]

$$L = (\mathscr{D}\sigma_e/\dot{\varepsilon}_e^C)^{1/3} \tag{4}$$

It is this parameter that governs the enhancement of grain boundary diffusion by creep around the cavity. With the assumption that the cavities retain their equilibrium caps characterized by the cavity tip angle ψ, the volumetric growth rate according to (1) leads to a rate of change of the cavity size according to $\dot{a} = \dot{V}/(4\pi a^2 h(\psi))$. Also, cavity growth gives rise to an increase of the average separation between the two adjacent grains, δ, i.e.

$$\dot{\delta} = \dot{V}/\pi b^2 \tag{5}$$

2.2. Mesoscopic model

The expressions mentioned above have subsequently been used in a microstructural model of HA in a multi-grain aggregate of grains [5, 6]. Each grain was represented separately and discretized using a rather fine finite element mesh to resolve the complex stress states in the grains (see Figure 2). Cavitation along the various grain boundary facets was accounted for through a cohesive zone model in terms of the average separation computed from the microscopic modelling according to (5). Primary interest at this scale was on the interaction between neighbouring cavitating facets under non-uniform distributions of methane pressure caused by distributions of different carbide types over the grain boundaries.

Studies for a range of material parameters and conditions have revealed that cavitation damage at this length scale can be idealized as one of the two cavitation modes. In one extreme mode, when the grains can creep significantly, the cavitation concentrates primarily on facets perpendicular to the macroscopic maximum principal stress. In the other mode, creep deformations of the grain are negligible and cavitation develops uniformly along all the facets. In either case, but most strongly in the latter, the stress state in the neighbourhood of the grain boundary cavities can be distinctly different from the macroscopic state of stress.

2.3. Macroscopic model

The observations in Reference [6] have been used next to guide the development of a continuum model for HA damage [7]. Ultimately, the corresponding constitutive equation for the macroscopic stress $\mathbf{\Sigma}$ reads

$$\overset{\nabla}{\mathbf{\Sigma}} = \mathscr{L} : (\mathbf{D} - \mathbf{D}^{CC} - \alpha\dot{T}\mathbf{I}) \tag{6}$$

where $^{\nabla}$ denotes the Jaumann derivative, $\mathbf{D}$ the macroscopic strain rate and $\mathbf{D}^{CC}$ the strain-rate contribution due to creep and grain boundary cavitation. $\mathscr{L}$ is the fourth-order tensor of

elastic moduli and α is the thermal expansion coefficient. If there were no cavitation, $\mathbf{D}^{CC}$ would simply be equal to the power-law creep rate

$$\mathbf{D}^{C} = \dot{E}_{e}^{C} \frac{3}{2} \frac{\mathbf{S}}{\Sigma_{e}} \tag{7}$$

with $\mathbf{S}$ the macroscopic stress deviator and $\dot{E}_{e}^{C}$ determined by the macroscopic effective stress Σ_{e} through (3). If there is cavitation, $\mathbf{D}^{CC}$ also accounts for the macroscopic rate of deformation caused by cavitation through the average separation rate $\dot{\delta}$ through (5). The way in which this is done depends on the mode of cavitation as mentioned in the previous section.

When creep deformations of the grains are significant, the effect of grain boundary cavitation can be described in terms of a penny-shaped crack model, similar to Tvergaard's [10] creep rupture model. In that case, $\mathbf{D}^{CC}$ is taken equal to

$$\mathbf{D}_{p}^{CC} = \dot{E}_{e}^{C} \left[\frac{3}{2} \frac{\mathbf{S}}{\Sigma_{e}} \left(1 + \rho \sum_{k=1}^{3} \left(\frac{n-1}{n+1} \right) \left(\frac{\boldsymbol{\Sigma} : \mathbf{m}_{k} - \sigma_{n,k}}{\Sigma_{e}} \right)^{2} \right) + \rho \sum_{k=1}^{3} \mathbf{m}_{k} \left(\frac{2}{n+1} \frac{\boldsymbol{\Sigma} : \mathbf{m}_{k} - \sigma_{n,k}}{\Sigma_{e}} \right) \right] \tag{8}$$

This expression accounts for the contribution of three orthogonal families of cavitating facets with unit normal vector $\mathbf{n}_{k}$ $(k = 1, \ldots, 3)$. The second-order tensor $\mathbf{m}_{k}$ is defined as $\mathbf{n}_{k} \otimes \mathbf{n}_{k}$ (no sum on k), so that $\boldsymbol{\Sigma} : \mathbf{m}_{k}$ is the component of the macroscopic stress deviator normal to grain facets in the kth direction. The parameter ρ is related to the density of cavitating facets, and is given by $\rho = 0.168(n+1)/\sqrt{1+3/n}$ when all are potentially cavitated. The $\sigma_{n,k}$ in (8) is the normal stress transmitted by the facets normal to the kth direction. This stress is determined from the condition that the cavitation rate $\dot{\delta}(\sigma_{n,k})$ caused by cavitation under a facet normal stress of $\sigma_{n,k}$ according to (1)–(5) should be equal to the opening rate $\dot{\delta}_{p,k}$ of a facet-size penny-shaped 'crack' (radius R) in a creeping solid bridged by the same stress,

$$\dot{\delta}_{p,k} = \frac{4}{\pi} \left(1 + \frac{3}{n} \right)^{-1/2} \frac{\boldsymbol{\Sigma} : \mathbf{m}_{k} - \sigma_{n,k}}{\Sigma_{e}} \dot{E}_{e}^{C} 2R \tag{9}$$

In the other extreme mode of deformation, where creep of the grains is negligible, the macroscopic strain rate is

$$\mathbf{D}_{rg}^{CC} = \dot{E}_{e}^{C} \frac{3}{2} \frac{\mathbf{S}}{\Sigma_{e}} + \kappa \frac{\dot{\delta}_{rg}}{R} \mathbf{I} \tag{10}$$

and consists of a pure (yet small) creep part and a dilatational part due to isotropic cavitation on all facets. The cavitation rate $\dot{\delta}_{rg}$ is equal to the separation rate from (1)–(5) with the facet normal stress being taken equal to the macroscopic hydrostatic stress $\Sigma_{m} = \boldsymbol{\Sigma} : \mathbf{I}/3$. The coefficient κ depends on the grain shape and is taken to be equal to 0.31 here.

The two extreme modes are combined simply by selecting one (8) or the other (10). The criterion used to select the mode is simply the maximum value of the cavitation rates predicted in each of the two modes. If $\dot{\delta}_{rg}$ delivers the largest value, $\mathbf{D}^{CC}$ to be substituted into (6) is taken to be equal to that in (10), otherwise the expression in (8) is used. To improve the numerical stability, a forward gradient approach is adopted to derive the rate tangent operator used in the integration of (6).

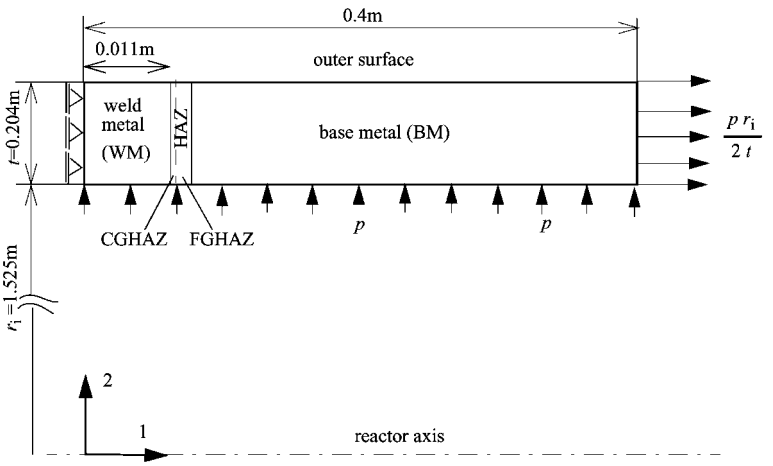

Figure 3. Axisymmetric model for a welded reactor containing four microstructural regions (WM, CGHAZ, FGHAZ and BM) showing its dimensions (not to scale), and boundary conditions.

3. APPLICATION TO A WELDED REACTOR

The macroscopic, continuum model is implemented in a finite strain, finite element model of a vessel containing a weldment and the gradual attack of the vessel until first failure is studied. Details may be found in Reference [11]. Thick-walled reactors are often manufactured by circumferential welding of forged belts made of 2.25Cr–1Mo steel. The four major microstructural regions in a weldment are: the weld metal (WM); the coarse-grained heat-affected zone (CGHAZ); the fine-grained heat-affected zone (FGHAZ); and the base metal (BM). These differ in grain size and probably in carbide type and composition, and possess different creep properties. Under creep conditions, welded components made of 2.25Cr–1Mo usually fail inside the fine-grained heat-affected zone [12].

As an example, we investigate the damage evolution in a welded reactor with an inner radius r_i of 1.525 m and a wall thickness t of 0.204 m (see Figure 3). Its circumferential weld is 0.022 m wide while the coarse-grained heat-affected zone (CGHAZ) and the fine-grained heat-affected zone (FGHAZ) have widths of 0.0006 and 0.0013 m, respectively. An axisymmetric finite element model is suitable to represent this welded reactor, where each of the four major microstructural regions of the weldment are represented separately. Due to symmetry it is sufficient to model half of the weldment. Therefore, symmetric boundary conditions are imposed along the middle line of the weld. At the other boundaries we prescribe tractions as illustrated in Figure 3. A uniform pressure is applied at the inner surface equal to the pressure p of the gas mixture inside the reactor. Axial stresses occur due to the action of the internal pressure on the end-caps of the reactor. These are prescribed at the right-hand boundary of the model as a uniform axial stress $\sigma_a = pr_i/2t$.

The studied reactor is filled with a hydrogen-containing gas mixture producing an internal pressure p of 14.3 MPa with 12.8 MPa being due to the hydrogen ($p_{H_2,i} = 12.8$ MPa). In agreement with current practice of narrow-gap welding, the weld angle is only a few degrees and this inclination is therefore neglected in the analysis. The reactor operates at a temperature

of $T_i = 733$ K. At the outer surface the temperature is 10 K lower ($T_o = 723$ K) and there is nearly no hydrogen ($p_{H_2,o} = 0$ MPa). Under steady-state conditions, the temperature and the hydrogen pressure vary in radial direction as follows:

$$T(r) = T_o - (T_o - T_i)\frac{\ln(r/r_o)}{\ln(r_i/r_o)} \tag{11}$$

$$p_{H_2}(r) = p_{H_2,o} - (p_{H_2,o} - p_{H_2,i})\frac{\ln(r/r_o)}{\ln(r_i/r_o)} \tag{12}$$

As the hydrogen pressure and the temperature vary, the methane pressure will also vary over the wall thickness.

The thermodynamic model mentioned above [3] can be used to calculate the methane pressure in dependence of the hydrogen pressure, and the compositions of the carbides and ferrite. The compositions of the carbides vary in the different regions of the weldment. The compositions we have used in the present computations are obtained in a joint European project on hydrogen attack [13]. As the M_7C_3 carbides in the FGHAZ are the last stable, most methane is generated in this region. The cavity pressure p_m reaches 230 MPa at the inner side of the reactor. The M_7C_3 carbide in the BM is the most stable, leading to a methane pressure of only 110 MPa. Note, however, that this is still a factor 10 higher than the hydrogen pressure.

Besides the carbide composition, the microstructural regions differ in grain size and creep properties which affects the damage evolution additionally. For the base metal, we apply the same material parameters as in Reference [14]. The grain size enters the damage model through the parameter R (see Eqs. (8)–(10)), and is taken to have values 48 μm in BM, 80 μm in WM, 150 μm in CGHAZ and 20 μm in FGHAZ. Creep tests performed on simulated coarse-grained and fine-grained heat-affected zones and on weld metal confirm that these regions possess different creep properties. Assuming that the creep exponent n is independent of the region ($n = 6.5$), we can relate the minimum creep rates to each other. Based on experimental results we use values of $B(T)$ in (3) for WM, CGHAZ and FGHAZ that are 1/2, 1/5 and 8 times that in BM.

The damage is characterized by the ratio of cavity radius a to half cavity spacing b. The initial cavity radius a_I and the average initial half spacing b_I are input data of the model. Due to a lack of the detailed data at the moment, we assume the same uniform initial damage in all regions: $a_I = 0.04$ μm and $b_I = 4$ μm, both equal to the values used in Reference [14]. The damage model describes the growth of voids on three orthogonal families of cavitating facets with unit normal vector $\mathbf{n}_k$ ($k = 1, 2, 3$) (see Eq. (8)). As the principal stress directions for the configuration in Figure 3 are largely aligned with the co-ordinate axes, we have chosen the normal vectors $\mathbf{n}_k$ to be parallel to the co-ordinate axes and constant during the process. The damage of cavities normal to the 1-direction (axial direction) is characterized by $(a/b)_1$, while $(a/b)_2$ and $(a/b)_3$ signify the damage state of facets normal to the 2-direction (radial direction) and the 3-direction (circumferential direction), respectively. At the beginning, these three families have the same damage state $(a/b)_1 = (a/b)_2 = (a/b)_3 = 0.01$. Due to the external stresses and cavity pressure, the voids grow, $(a/b)_k$ increases until cavity coalescence takes place at $(a/b) \approx 0.7$, at which point the computation is stopped.

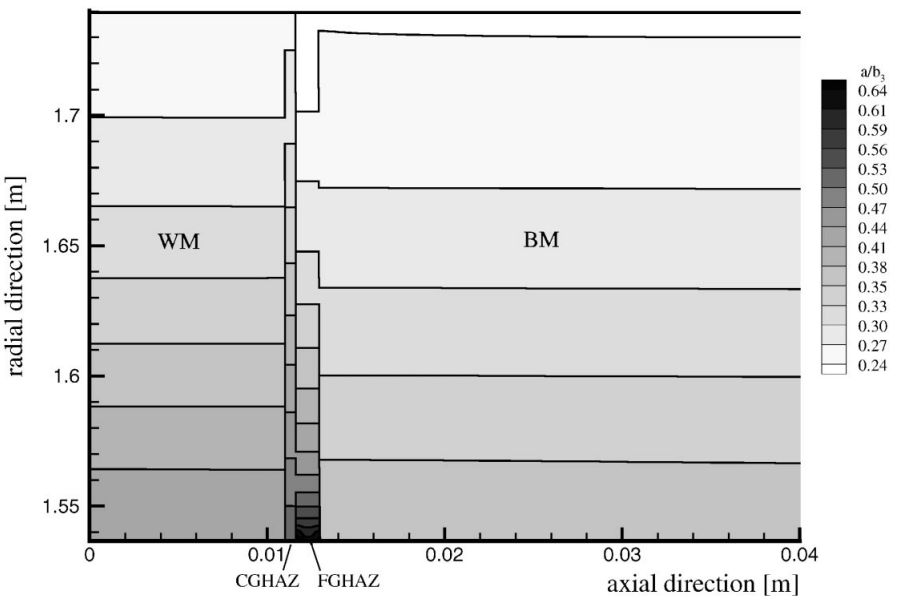

Figure 4. Damage distribution near the weldment on facets normal to the circumferential direction.

The finite element calculations give us the damage state in all regions at various times. In Figure 4 we show contours of damage at the instant of first cavity coalescence. The damage variable plotted is the value of $(a/b)_3$ on facets normal to the circumferential direction. It is seen that at this stage most damage occurs in FGHAZ, somewhat less in CGHAZ, followed by WM while BM shows the least damage. The regions differ in various respects, but closer examination of the results reveals that the difference in methane pressure is the main origin of the different damage states. The facets normal to the circumferential direction grow fastest due to the fact that the external stress component in the circumferential direction is much larger than the axial one and especially the radial one. Nevertheless, significant damage also occurs in the other directions which is the result of the cavity pressure.

The corresponding time at which coalescence is found to occur first in FGHAZ near the inner surface is roughly 26 years. This means that the model predicts a failure time of 26 years for a welded reactor with the mentioned material properties under the described operation conditions.

The computations also reveal that the damage process is accompanied by severe stress redistributions, especially in FGHAZ and CGHAZ. Due to the high methane pressure, the FGHAZ is damaged most, but the related expansion is constrained by the neighbouring CGHAZ which is damaged less and which has a significantly lower creep rate. As a consequence, load shedding takes place from the inner region of the vessel to the outer radius. The redistribution can be so strong that compressive stresses develop in the FGHAZ near the inside of the reactor. Evidently, this has dramatic consequence on the predicted time to coalescence, and exemplifies earlier suggestions [14] that lifetime predictions in these situations cannot be based on stress states corresponding to steady creep.

4. CONCLUSIONS

A continuum model for hydrogen attack at elevated temperatures and a typical application have been discussed. The model is motivated by consideration of the physical processes involved on three length scales. The transitions from one scale to the next cannot be carried out by analytical homogenization, because of the severe non-linearities involved. Rather, the numerical results at the smaller scale are captured in relatively simple observations that can be formulated in approximate relationships for the key quantities, which could then be used in the computational model at the next scale.

A significant simplification in the modelling was achieved by decoupling the description of the methane formation from that of the damage accumulation. This is consistent with the conventional view (e.g. References [2, 15]), but there are indications that need to be investigated in further detail. A more complete description would require a coupled modelling that accounts for the kinetics of the chemical reaction to methane, the dissolution of the carbides, the necessary diffusion processes as well as cavity growth by creep and grain boundary diffusion.

REFERENCES

1. Tvergaard V. Material failure by void growth to coalescence. *Advances in Applied Mechanics* 1990; **27**:83–151.
2. Sundararajan G, Shewmon PG. The kinetics of hydrogen attack of steels. *Metallurgical Transactions A* 1981; **12**:1761–1775.
3. Schlögl SM, van Leeuwen Y, van der Giessen E. On methane generation and decarburization in low alloy Cr–Mo steels during hydrogen attack. *Metallurgical and Materials Transactions A* 2000; **31**:125–137.
4. van der Burg MWD, van der Giessen E, Brouwer RC. Investigation of hydrogen attack in 2.25 Cr–1Mo steels with a high triaxiality void growth model. *Acta Materialia* 1996; **44**:505–518.
5. van der Burg MWD, van der Giessen E. Hydrogen attack in creeping polycrystals due to cavitation on grain boundaries. In *Proceedings of the Fifth International Conference on the effects of Hydrogen on Material Behavior*, Thompson AW, Moody NR (eds). TMS: PA, 1994; 313–323.
6. van der Burg MWD, van der Giessen E. Non-uniform hydrogen attack cavitation and the role of interaction with creep. *Materials Science and Engineering A* 1996; **220**:200–214.
7. van der Burg MWD, van der Giessen E. A continuum damage relation for hydrogen attack cavitation. *Acta Materialia* 1997; **45**:3047–3057.
8. van der Giessen E, van der Burg MWD, Needleman A, Tvergaard V. Void growth due to creep and grain boundary diffusion at high triaxialities. *Journal of Mechanics and Physics of Solids* 1995; **43**:123–165.
9. Needleman A, Rice JR. Plastic creep flow effects in the diffusive cavitation of grain boundaries. *Acta Metallurgica* 1980; **28**:1315–1332.
10. Tvergaard V. Constitutive relations for creep in polycrystals with grain boundary cavitation. *Acta Metallurgica* 1984; **32**:1977–1990.
11. Schlögl SM, van der Giessen E. Hydrogen attack in a welded reactor. *Journal de Physique IV* 1999; **9**:137–146.
12. Brett SJ. Cracking experience in steam pipework welds in national power. *VGB Conference Materials and Welding Technology in Power Plants 1994*, Essen, 15–16 March 1994.
13. Manolatos P. *Unpublished Research*. Joint Research Center, Petten, The Netherlands, 1999.
14. van der Burg MWD, van der Giessen E, Tvergaard V. A continuum damage analysis of hydrogen attack in a 2.25 Cr–1Mo vessel. *Materials Science and Engineering A* 1998; **241**:1–13.
15. Parthasarathy TA, Shewmon PG. Effects of tempering on the carbon activity and hydrogen attack kinetics of 2.25 Cr–1Mo steel. *Metallurgical Transactions A* 1984; **15**:2021–2027.

